Journal of ELECTRONIC MATERIALS, Vol. 47, No. 7, 2018
https://doi.org/10.1007/s11664-018-6195-8

Effects of a Thin Ru-Doped PVP Interface Layer on Electrical Behavior of Ag/n-Si Structures

YOSEF BADALI,[1,5] AFSOUN NIKRAVAN,[2] ŞEMSETTIN ALTINDAL,[3] and İBRAHIM USLU[4]

1.—Department of Advanced Technologies, Institute of Science and Technology, Gazi University, 06500 Ankara, Turkey. 2.—Department of Environmental Engineering, Institute of Science, Hacettepe University, 06800 Ankara, Turkey. 3.—Department of Physics, Faculty of Science, Gazi University, 06500 Ankara, Turkey. 4.—Department of Chemistry Education, Faculty of Education, Gazi University, Ankara 06500, Turkey. 5.—e-mail: bedeli.yusuf@gmail.com

The aim of this study is to improve the electrical property of Ag/n-Si metal–semiconductor (MS) structure by growing an Ru-doped PVP interlayer between Ag and n-Si using electrospinning technique. To illustrate the utility of the Ru-doped PVP interface layer, current–voltage (*I–V)* characteristics of Ag/n-Si (MS) and Ag/Ru-doped PVP/n-Si metal–polymer–semiconductor (MPS) structures was carried out. In addition, the main electrical parameters of the fabricated Ag/Ru-doped PVP/n-Si structures were investigated as a function of frequency and electric field using impedance spectroscopy method (ISM). The capacitance–voltage (*C–V*) plot showed an anomalous peak in the depletion region due to the special density distribution of interface traps/states (D_{it}/N_{ss}) and interlayer. Both the values of series resistance (R_s) and N_{ss} were drawn as a function of voltage and frequency between 0.5 kHz and 5 MHz at room temperature and they had a peak behavior in the depletion region. Some important parameters of the sample such as the donor concentration atoms (N_D), Fermi energy (E_F), thickness of the depletion region (W_D), barrier height (Φ_{B0}) and R_s were determined from the C^{-2} versus V plot for each frequency. The values of N_D, W_D, Φ_{B0} and R_s were changed from 1×10^{15} cm^{-3}, 9.61×10^{-5} cm, 0.94 eV and 19,055 Ω (at 0.5 kHz) to 0.13×10^{15} cm^{-3}, 27.4×10^{-4} cm, 1.04 eV and 70 Ω (at 5 MHz), respectively. As a result of the experiments, it is observed that the change in electrical parameters becomes more effective at lower frequencies due to the N_{ss} and their relaxation time (τ), dipole and surface polarizations.

Key words: Electrical characteristics, Ru-doped PVP, surface states, series resistance

INTRODUCTION

Among the various organic materials (polymers), polyvinyl alcohol (PVA), polyaniline/pyrrole/thiophene and polyvinyl carbonate/pyrrolidone have become appealing research topics for chemists, physicists and electronic engineers because of their attractive properties. Especially, polyvinyl pyrrolidone (PVP) has important properties such as having a high dielectric constant, good workability, high charge storage ability and a moderate electrical conductivity and charge transfer mechanism. The PVP is an amorphous polymer and has high glass transition temperature (T_g) due to the existence of the rigid pyrrolidone group which varies from different complexes to inorganic salts.[1–3] There are a considerable number of early modern studies in semiconductor physics directed to the manufacture of metal–semiconductor (MS) structures with a new interfacial layer for reducing

(Received November 17, 2017; accepted March 1, 2018; published online March 12, 2018)

the transition energy or band gap.[4,5] Ruthenium (Ru) is also an attractive element due to its promising characteristics such as low resistance (7.1×10^{-6} Ω cm for Ru and 30.0×10^{-6}Ω cm for RuO_2) and a high work function [4.6 eV for Ru and 5.1 eV for ruthenium oxide (RuO_2)].[6,7] Recently, many researchers have focused on RuO_2 due to its excellent electrochemical and photochemical catalysis properties as well as its excellent load storage feature.[8] In addition, various applications of Ru such as ferroelectric random-access memories (FERAMs), metal-oxide semiconductor field effect transistors (MOSFETs) and being a seed layer for copper interconnections increase its significance.

Moreover, there has recently been an increase in the interest in the deposition of metallic Ru films as well as RuO_2 films. Ru is used as an adhesive layer for a diffusion barrier as well as an electrode for dynamic random-access memories (DRAMs).[9–11] Other applications for Ru thin films are used in very large-scale integration (VLSI) capacitor-based high-dielectric materials as a bottom electrode.[11–14]

Some studies found electrospinning to be unique in producing uninterrupted nanofibers with lengths of several meters, ease of manufacture and compliance.[3,4] This method utilizes electrostatic force to produce polymer fibers and it has four major components: (a) a power supply with high voltage, (b) a spinner, (c) a syringe pump and (d) a metal collector. Some chemical and physical parameters such as viscosity of the polymer solution, electrical conductivity and concentration of doped materials directly influence the formability and shaping of electrospun fibers.[3,4] Moreover, some other studies show that forming very fine nanofibers on a semiconductor wafer positively affects the performance of Schottky structures.[15] The growing of such polymer layers at the MS interface causes this structure to convert into the metal–polymer–semiconductor (MPS) structure which stores dielectric charge due to the dielectric properties of the interface layer.

In this study, to enhance the performance of Ag/n-Si (MS) structure, Ru-doped PVP was used as an interlayer between Ag and the silicon wafer (Fig. 1a), due to its simple processing and compatibility with silicon. After ohmic contact, Ru-doped PVP thin film was formed in front of the silicon wafer by electrospinning method. In order to see the effect of Ru-doped PVP insulators layer on the electrical behavior of Ag/n-Si MS structure, the *I–V* features of Ag/n-Si and Ag/Ru-doped PVP/n-Si structures were investigated. In addition, the influence of N_{ss}, R_s and Ru-doped PVP interface layer on the prepared structure was investigated. To this end, both the R_s-*V* and N_{ss}-*V* plots and R_s-log*f* and N_{ss}-log*f* for various voltages were obtained by using *C* and *G* data between 0.5 kHz and 5 MHz at room temperature. Finally, some important electronic parameters of the prepared sample such as N_D, E_F, W_D and Φ_{B0} were obtained from the inversion region of C^{-2} versus *V* plots for each frequency.

EXPERIMENTAL PROCEDURES

In this study, an Ag/Ru-doped PVP/n-Si device was fabricated using *n*-type silicon [n-Si, (100)] wafer with 300-μm thickness and 1–10-Ω cm resistance as a substrate. The n-Si was chemically cleaned in an ultrasonic bath using acetone and isopropyl alcohol for 5 min and then quenched in high-resistance (18 Ω) deionized water for a prolonged time. Finally, they were dried with pure, dry nitrogen gas. Then, 100-nm-thick high-purity (99.999%) silver (Ag) dots were thermally evaporated onto the backside of Si. To form a low-resistance ohmic contact, they were annealed at 450°C for 3 min in nitrogen (N_2). After these processes, the native oxide on the surface of Si was removed by using HF:10H_2O solution and then it was rinsed in deionized water for 30 s and dried with N_2.

Ruthenium (III) 2,4-pentanedionate was supplied from Alfa-Aesar and PVP (MW 40,000) was supplied by Sigma-Aldrich. At first, an aqueous PVP solution (20 pct w/w) was prepared by dissolving the PVP in ethanol. It was stirred at 80°C for 2 h by using a magnetic stirrer, and then the temperature of the solution was reduced to room temperature. The ruthenium (III) 2,4-pentanedionate dopant was added to the prepared solution with a molar concentration of 3%. The solution was vigorously stirred for 2 h at 60°C by means of a magnetic stirrer to yield a clear and homogeneous solution. The prepared Ru-doped PVP sol–gel was deposited as a nanofiber thin layer on Si substrate by using the electrospinning technique. The electrospinning setup includes four main parts: (1) the syringe, (2) the high-voltage supply, (3) the infusion pump and (4) the collector material. As a typical procedure, by using an infusion syringe pump, the polymer solution was pumped through the tube to a metal needle syringe ("nozzle", 5 ml) with an inner diameter of 0.30 mm at a fixed flow rate of 0.01 ml/h. The needle was positioned horizontally on the syringe pump and connected to a high-voltage power supply. In order to collect the nanofibers, a piece of Si was placed 17 cm from the tip. After applying a high-bias V as 15 kV on the tip, an electric field was created to help eject a fluid jet from the nozzle. After the formed fiber was dried in vacuum for 8 h at 85°C, the solvent was evaporated and nanofiber film on Si wafer was coated as a non-woven material. In order to perform rectifier contacts, the high-purity Ag (99.999%) was coated on the Ru-doped PVP with a 7.85×10^{-3}-cm^2 contact area and 1500 Å in the high-vacuum metal evaporation system. Thus, the manufacturing process of Ag/Ru-doped PVP/n-Si structure was completed. All evaporation and coating processes were performed in a high-vacuum

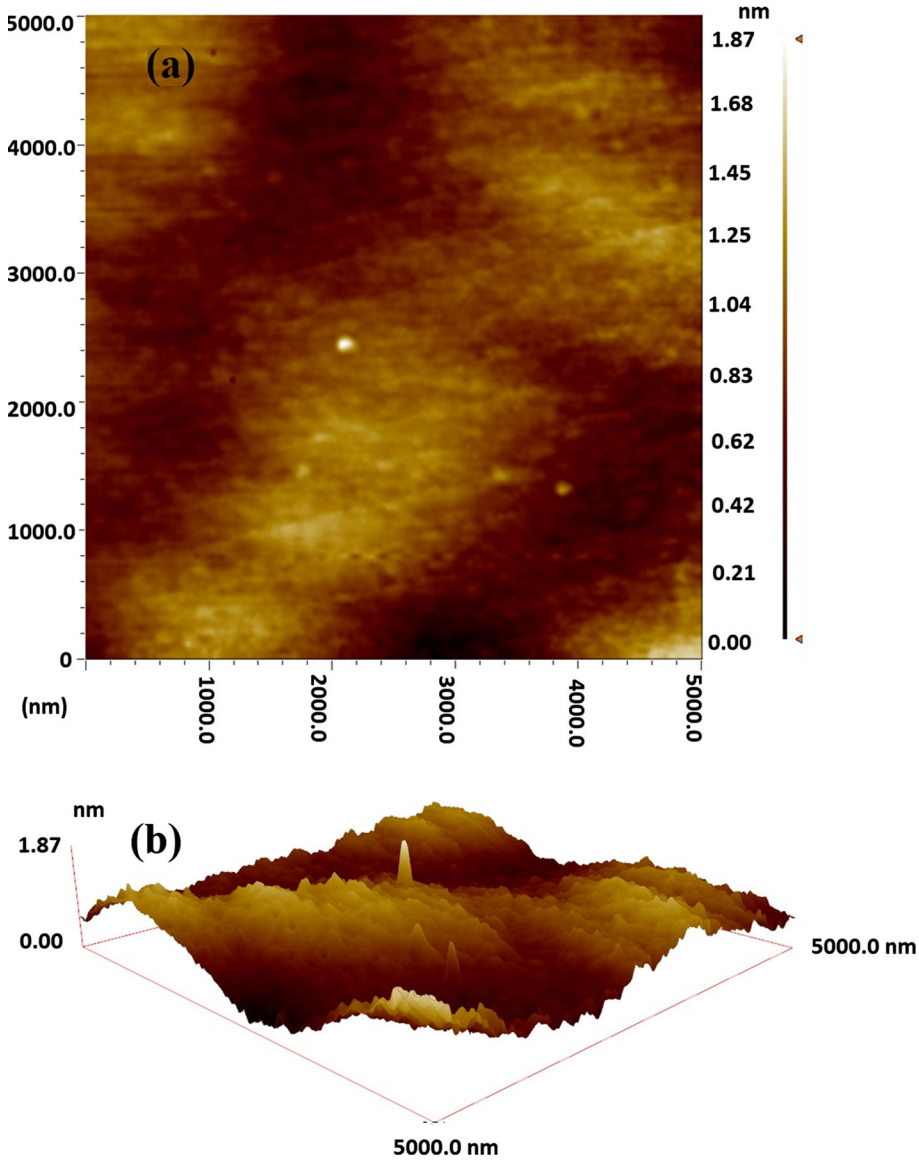

Fig. 1. Atomic force microscopy (AFM) images of Ru-doped PVP structure: (a) two-dimensional and (b) three-dimensional.

metal evaporation unit at about 5.3×10^{-7} kPa at a rate of 4 Å/s using a metal shadow mask.

EXPERIMENTAL RESULTS AND DISCUSSION

Morphological Analysis

The surface morphology of the electrospun Ru-doped PVP with a 5 x 5 μm^2 surface area was characterized by using the non-contact mode of atomic force microscopy (AFM). Figure 1 presents the two- (2D) and three-dimensional (3D) AFM images of the Ru-doped PVP surface. The surface roughness included various roughness parameters such as average roughness (R_a), surface skewness (R_{sk}), root mean square roughness (RMS) and surface kurtosis (R_{ku}). RMS and average roughness values of the sample were obtained as 7.62 nm and 4.32 nm, respectively, over a scan area of 5 x 5 μm^2. R_{sk} was a measure of height distribution symmetry and obtained for this sample as 0.038. This value suggests that the peaks dominated the surface and, therefore, the surface of the fibers was nonporous. R_{ku} describes sharpness of the height distributions and a value of 2.35 was obtained for this sample, indicating a flat and repetitive surface.[16]

The scanning electron microscopy (SEM) images of the formed fibers and their diameter distributions are given in Fig. 2a and b, respectively. The SEM images reveal important information about the fiber structure of Ru-doped PVP materials such as homogeneity, bead formation and fiber diameters. Figure 2a illustrates the bead-free, smooth and interconnected structure of the nanofibers. Figure 2 confirms that the Ru-doped PVP film successfully deposited on the Si surface concluded to uniform

fibers with a wide distribution of the fiber diameters. The average diameter distribution of the fibers was found as 127.68 nm and most fiber diameters are between 60 nm and 180 nm, as shown in Fig. 2b. This result shows that the majority of the fibers were formed in nanoscale.

Current–Voltage Characteristics

To illustrate the utility of the Ru doped PVP interface layer, semi-logarithmic *I–V* characteristics of Ag/n-Si MS and Ag/Ru-doped PVP/n-Si MPS structures were drawn and shown in Fig. 3. The forward-bias semi-logarithmic *I–V* plots for the two structures show a linear behavior in the intermediate biases which then considerably deviates from the linearity at sufficiently high bias voltage due to the effect of series resistance (R_s) and an interfacial native layer (SiO_2) or deposited Ru-doped PVP (Fig. 3). The reverse-bias *I–V* characteristics indicated good saturated behavior or were independent of voltage. Their *I–V* characteristics at $V \geq 3kT/q$ were analyzed based on thermionic emission (TE) theory. It is known that when a Schottky-type structure has an R_s and ideality factor (n) values higher than unity, the forward-bias *I–V* characteristics can be communicated with.[17,18]

$$I = AA^*T^2 \exp\left(-\frac{q}{kT}\Phi_{Bo}\right)\left[\exp\left(\frac{q(V-IR_s)}{nkT}\right)-1\right] = I_0\left[\exp\left(\frac{qV_D}{nkT}\right)-1\right] \quad (1a)$$

In this equation, the quantities of I_o, A^*, Φ_{Bo}, V_D and T are the reverse-bias saturation current, effective Richardson constant, zero-bias or apparent barrier height (BH), voltage drop across the diode and temperature, respectively. The values of I_o and n were obtained from the intercept and slope of Ln(I)–V plots by using the relation and neglecting both the R_s and last term in Eq. 1a.

$$Ln(I) = Ln(I_o) + qV/nkT \quad (1b)$$

The value of Φ_{Bo} is obtained using a theoretical value of A^* and extrapolating I_o values following the equation.[17,18]

$$\Phi_{Bo} = \frac{kT}{q}\ln\left(\frac{A \cdot A^*T^2}{I_o}\right) \quad (2)$$

The values of the series and shunt resistance (R_s and R_{sh}) were obtained from Ohm's law ($R = dV/dI$) at sufficient forward- and reverse-bias voltages (± 5 V), respectively. The acquired experimental values of I_o, n, Φ_{B0}, R_s, R_{sh} and rectifying rate (RR) for MS and MPS structures are presented in Table I. While the values of I_o, n and R_s for MS structure is higher than MPS structure, Φ_{Bo}, R_{sh} and RR are lower for MS structure due to the

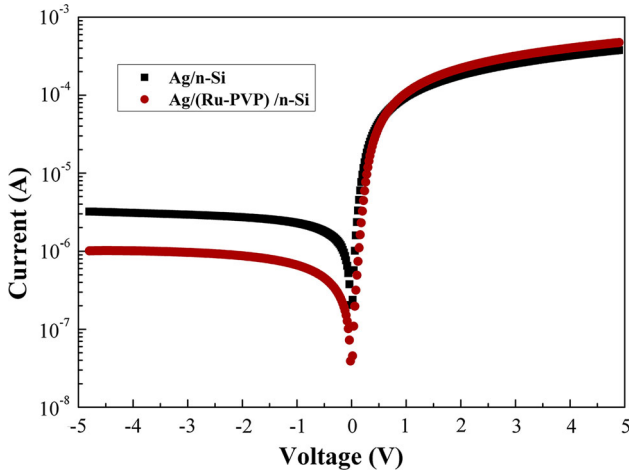

Fig. 3. The *I–V* plots of the Ag/n-Si and Ag/Ru-doped PVP/n-Si structures at room temperature.

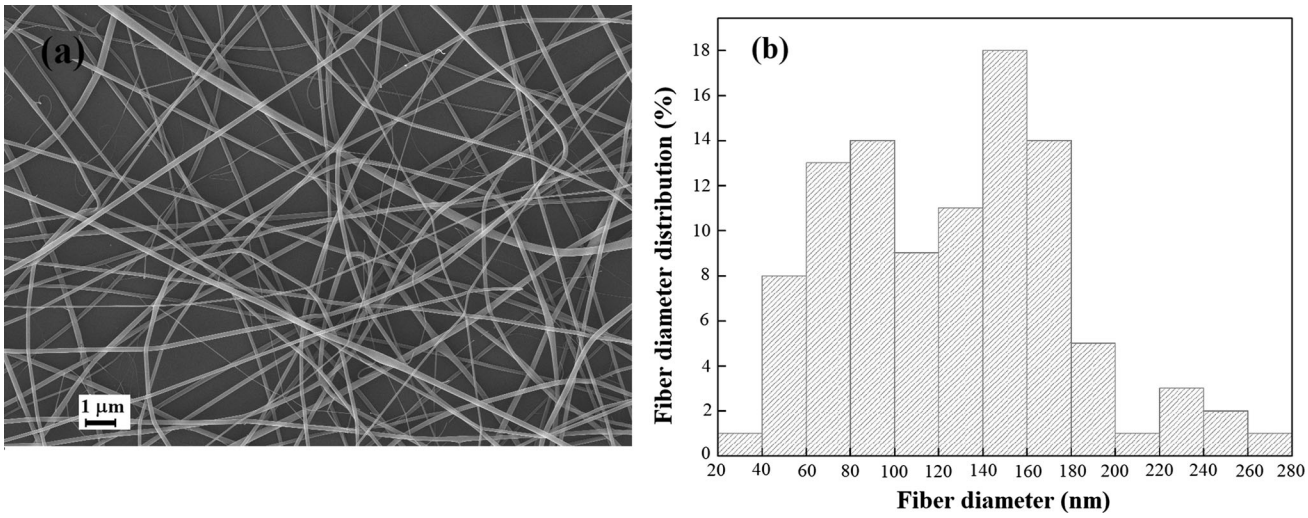

Fig. 2. (a) Scanning electron microscopy image. (b) diameter distributions of Ru-doped PVP fibers.

decrease in the electron tunneling at the Ru-doped PVP–n-Si interface and decrease in the leakage current (Table I and Fig. 3). Therefore, these interfacial layers formed a physical barrier between the metal and semiconductor that prevented the reaction and interdiffusion between Ag and n-Si. For instance, the value of RR for MPS structure (490) was almost 11 times higher than the MS structure (43.3). Moreover, compared to the MS structure, the value of n for MPS was smaller and closer to unity because of the passivation effect of the interfacial Ru-doped PVP layer. These experimental results confirmed that the Ru-doped PVP interlayer enhances the performance of Ag/n-Si structure. This is because the Ru incorporation in PVP lattices reduces the oxygen vacancies and therefore decrease the density of surface states (N_{ss}) that can effectively increase the BH of an MPS structure.[19]

The high values of n for two types of diodes (Table I) are attributed to the special density distribution of the surface states, the image-force lowering effect, recombination-generation, tunneling through the barrier and inhomogeneities of BH at the MS interface.[18,20,24] Equation 3a shows that the value of n is dependent on the doping level of concentration atoms or depletion layer width (W_d). In addition, barrier in-homogeneities at the MS interface leads to an increase in n because the BH shape is not flat and it has many lower barriers, pinch-off or patches at an approximately mean BH.[20,24] Thus, some carriers with lower energy from the mean BH can easily pass over these lower barriers and yield an increase of current, thus leading to an increase of current and an increase of n. The values of n and Φ_{Bo} are approximately related to the applied bias voltage after the linear region as in the following equations:

$$n(V) = \frac{qV}{kT \cdot Ln(I/I_o)} = 1 + \frac{\delta}{\varepsilon_i}\left[\frac{\varepsilon_s}{W_D} + qN_{ss}(V)\right] \quad (3a)$$

$$\Phi_e = \Phi_{Bo} + \alpha(V) = \Phi_{Bo} + \left(1 - \frac{1}{n(V)}\right)V \quad (3b)$$

In these equations, $\alpha\,[\alpha = d\Phi_e/dV = 1 - 1/n(V)]$ is the voltage-dependent coefficient of BH, ε_s and ε_i are the permittivity of the semiconductor and insulator layer, respectively.

During the elaboration of semiconductor devices such as MS or metal–insulator–semiconductor (MIS)/MPS structures, many defects may occur at the MS interface with energy states located in the forbidden band gap of the semiconductor. These traps may originate from interruption of the periodic lattice structure or disorder at the crystal's surface with energy states in the forbidden band gap. Therefore, surface states and dislocations are usually dependent on the chemical composition of the interface.[20,24] When interfacial layer is thick enough (≥ 30 Å), these surface states are in equilibrium with the semiconductor and they are defined by the change in energy of the states relative to the Fermi energy level in the semiconductor.[20] Moreover, when interface layer thicknesses are lower than 30 Å, the surface states are in equilibrium with the metal. The schematic of the energy band diagram of the Au/Ru-doped PVP/n-Si structure is given in Fig. 4. This figure shows the location of surface states in the interface layer.

Equation 4a gives the energy of interface states (E_{ss}) that can be estimated with respect to the conduction band (E_c) of the n-type semiconductor.

$$E_c - E_{ss} = q\,(\Phi_e - V) \quad (4a)$$

In this way, the energy density distribution of N_{ss} was measured by using the Card-and-Rhoderick method as in 4b[20]:

$$N_{ss}(V) = 1/q\,[\varepsilon_i/\delta(n\,(V) - 1) - \varepsilon_s/W_D] \quad (4b)$$

Figure 5 shows the energy density distribution of N_{ss} for the Ag/n-Si MS structure with and without an Ru-doped PVP interfacial polymer layer at room temperature. The values of N_{ss} for Ag/Ru-doped PVP/n-Si structure are considerably low compared with Ag/n-Si structure, especially near the E_c edge (Fig. 5). These results verified that Ru-doped PVP interlayer improves the performance of Ag/n-Si structure.

Capacitance/Conductance/Voltage Characteristics

The analysis of the impedance spectroscopy method, including a series of the forward and reverse C–V and $G/$–V measurements, may provide more detailed knowledge about electrical characteristics. Therefore, the C–V and $G/$–V measurements of the Ag/Ru-doped PVP/n-Si structure were performed in a wide frequency range (0.5 kHz–5 MHz) and applied bias voltage (± 5 V) at room temperature (Figs. 6 and 7). It is clear that both the C–V and $G/$–V plots have inversion, depletion and

Table I. Electrical parameters of Ag/n-Si and Ag/Ru-doped PVP/n-Si structures at room temperature

Samples	Io (A)	n	Φ_{Bo} (eV)	R_s (Ω)	R_{sh} (Ω)	RR
Ag/n-Si	5.92×10^{-7}	2.84	0.69	3.56×10^{4}	1.54×10^{4}	43.3
Ag/Ru-doped PVP/n-Si	8.01×10^{-8}	1.93	0.75	1.04×10^{4}	5.10×10^{4}	490

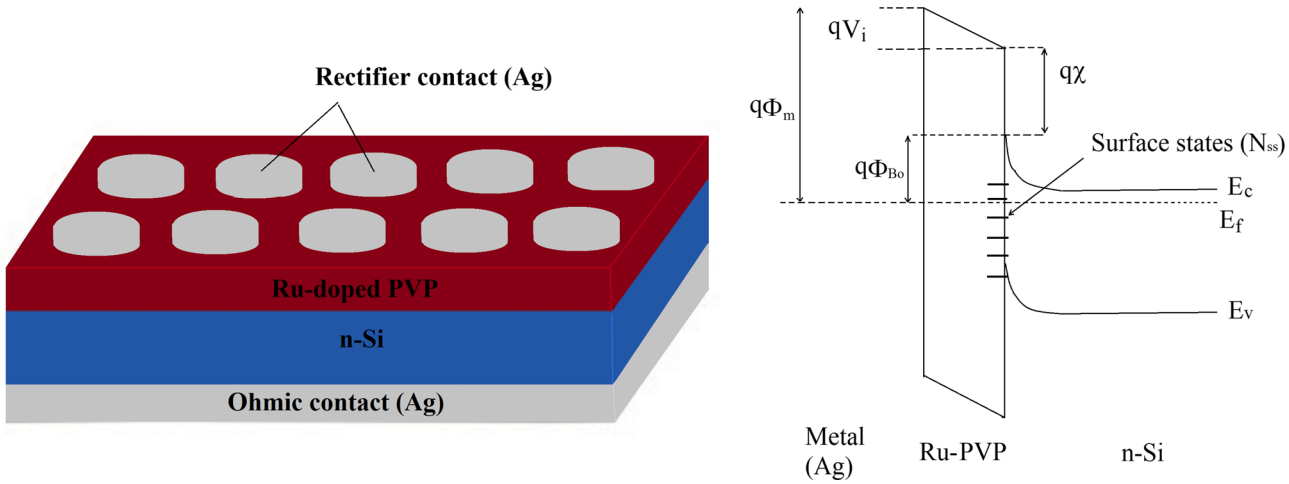

Fig. 4. The schematic and energy band diagram of the Au/Ru-doped PVP/n-Si structure.

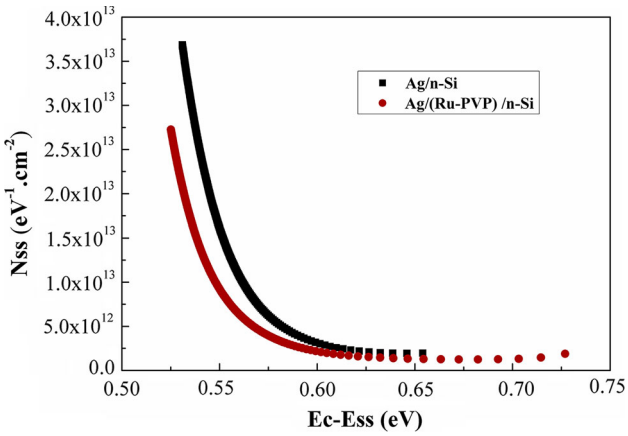

Fig. 5. The energy density distribution profile of N_{ss} for the Ag/n-Si and Ag/Ru-doped PVP/n-Si structures at room temperature.

accumulation regions like an MIS or MOS type structures. In the ideal case, the values of C and G/w should be independent of the frequency, but the status is considerably different for this structure (Figs. 6 and 7). The discrepancy in C–V and G/w–V characteristics becomes large in the depletion and the accumulation region, especially at low frequencies due to the existence of charges at states or traps localized at the Ru-doped PVP/n-Si interface, their relaxation time (τ) and surface polarization. The changes in the C and G/w values are considerably low, but after at about 10 kHz, they start to decrease with increasing frequency rapidly for each bias voltage in the accumulation region (shown as an inset in Figs. 6 and 7) due to the effect of R_s. In addition, both the C–V and G/w–V plots have a peak in the depletion region at low frequencies due to N_{ss} and their position shifts towards the positive bias region with decreasing frequency. As known, at lower frequencies, surface states or traps can easily follow the ac signal and this causes a storage of excess capacitance ($C_{ex.}$) and conductance ($G_{ex./}$).

In general, the values of N_{ss} and R_s of the Ag/Ru-doped PVP/n-Si structure is responsible for an anomalous bias of the C–V and $G/$ characteristics. While the N_{ss} is especially effective in the depletion and inversion regions, R_s are effective only in the accumulation region. Thus, the voltage-dependent profile of R_s was obtained by using Nicolai and Brew's method,[21] which provides the determination of R_{est} in the whole voltage range and is given as:

$$R_s = \frac{G_m}{G_m^2 + {}^2\, C_m^2} \tag{5}$$

where C_m and G_m are the obtained values of capacitance and conductance for any applied bias voltage, respectively. Thus, the voltage-dependent profile of R_s of the Ag/Ru-doped PVP/n-Si structure were calculated from the measured C and G data for each frequency (Fig. 8). It was observed that the value of R_s decreases with increasing frequency for each applied bias voltage, but the real value of R_s corresponds to the accumulation region ($-$ 5 V) at enough high frequencies (f $\geq$ 1 MHz). The high values of R_s at low frequencies are the result of N_{ss}, but at sufficiently high frequencies (f $\geq$ 1 MHz), they do not contribute directly to the total of R_s.

To obtain the frequency-dependent conduction mechanisms of the Ag/Ru-doped PVP/n-Si structure, C^{-2}–V plots were drawn (Fig. 9). These plots show straight lines in the wide voltage region (0.3–2.8 V). In the MIS- or MPS-type structures, the values of the depletion layer capacitance vary with the applied bias voltages (V) expressed as (6)[21–25]:

$$C^{-2} = \frac{2}{q\varepsilon_s\varepsilon_o N_D A^2}(V_D - kT/q - V) \tag{6}$$

where N_D is the concentration of doping donor atoms (P), V_D is the diffusion potential, A is the rectifier contact area, ε_s (ε_s = 11.8ε_o) and ε_o are the permittivity of the semiconductor and vacuum,

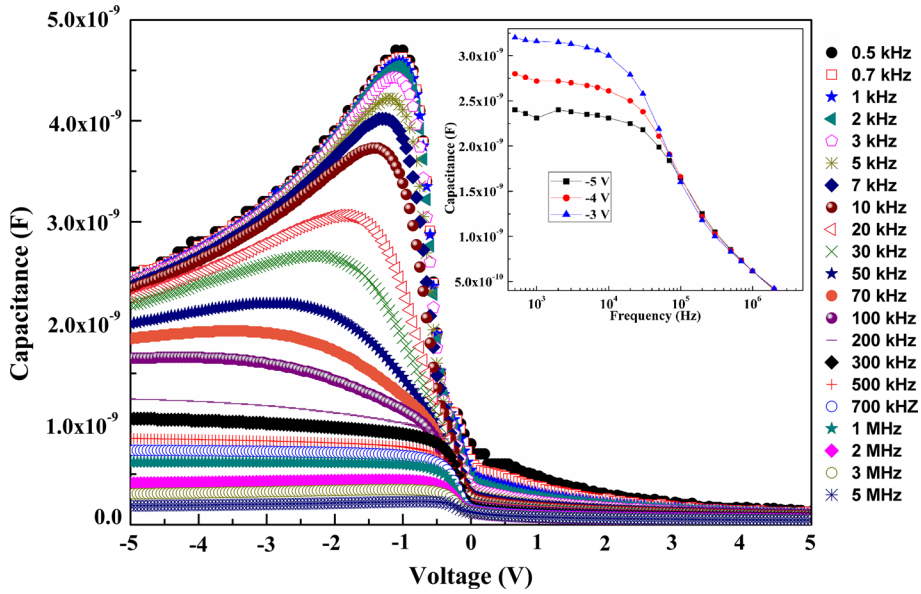

Fig. 6. The forward- and reverse-bias *C–V* plots of the Ag/Ru-doped PVP/n-Si structure for various frequencies at room temperature. Inset: The C–*f* plots of the Ag/Ru-doped PVP/n-Si structure for various voltages.

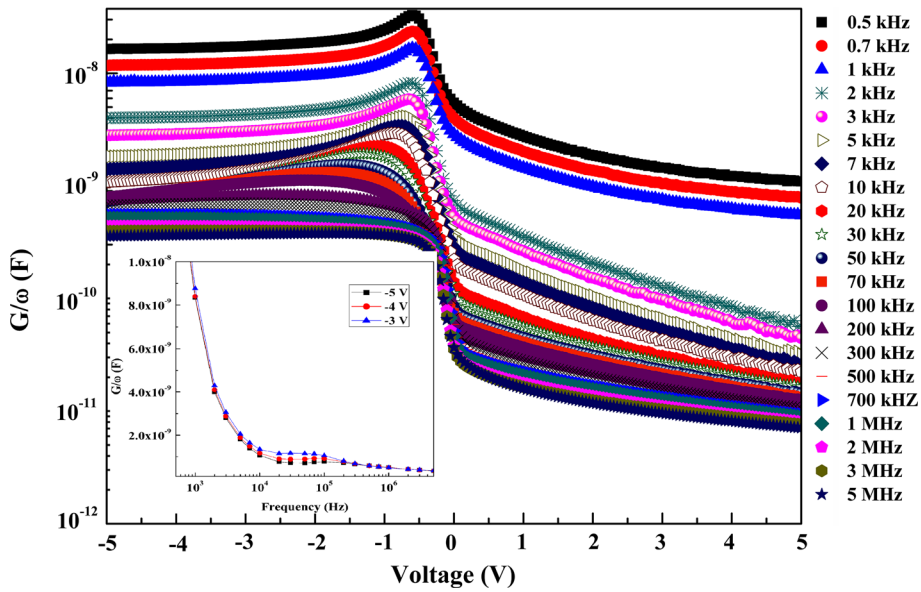

Fig. 7. The forward- and reverse-bias *G/–V* plots of the Ag/Ru-doped PVP/n-Si structure for various frequencies at room temperature. Inset: The *G/–f* plots of the Ag/Ru-doped PVP/n-Si structure for various voltages.

respectively. Thus, some main electrical parameters of the structure such as V_D, N_D, Fermi energy level (E_F), maximum electric field (E_m), W_d) and BH (Φ_{C-V}) were obtained from the intercept, and the slopes of the C^{-2} versus V plot for each frequency are presented in Table II. The voltage intercept of the C^{-2} versus V plot at zero bias gives V_o which is related to V_D (D = $V_o + kT/q$). The values of N_D were obtained from the slope of the linear part of the C^{-2}–V plot. Subsequently, the value of E_F was also obtained for each frequency by using the following relations (7a and b).

$$E_F = \frac{kT}{q}\ln\left(\frac{N_C}{N_D}\right) \tag{7a}$$

with

$$N_C = 4.82 \times 10^{15} T^{3/2} (m_e^*/m_0)^{3/2} \tag{7b}$$

where N_C is the effective density of states in the conduction band of Si (E_c), $m_e^* = 0.98\,m_0$ is the effective mass of the electron[24] and m_o (9.1×10^{-31} kg) is the rest mass of the electron. The value of image-force lowering of the BH ($\Delta\Phi_B$) and the

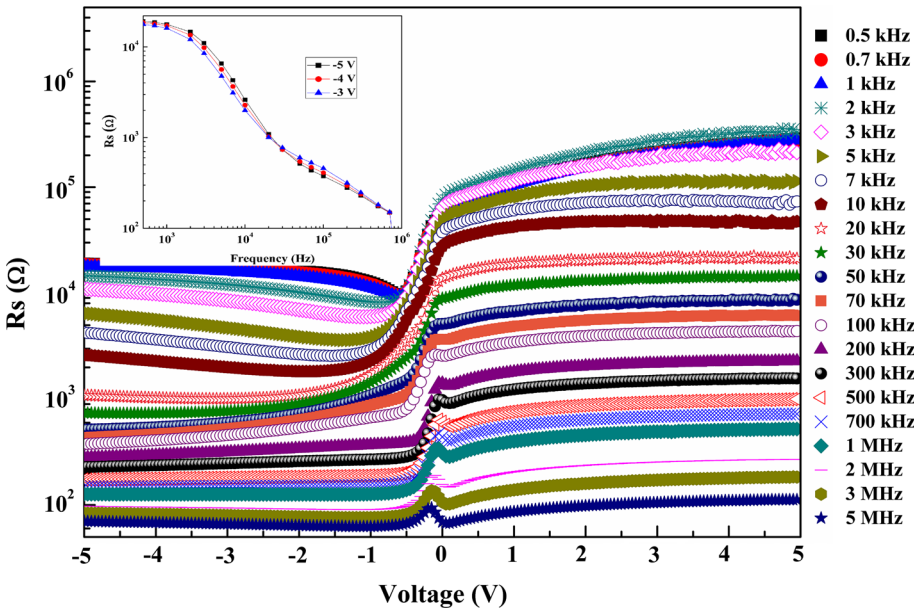

Fig. 8. The R_s–V plots of the Ag/Ru-doped PVP/n-Si structure for various frequencies at room temperature. Inset: The R_s–f plots of the Ag/Ru-doped PVP/n-Si structure for various voltages.

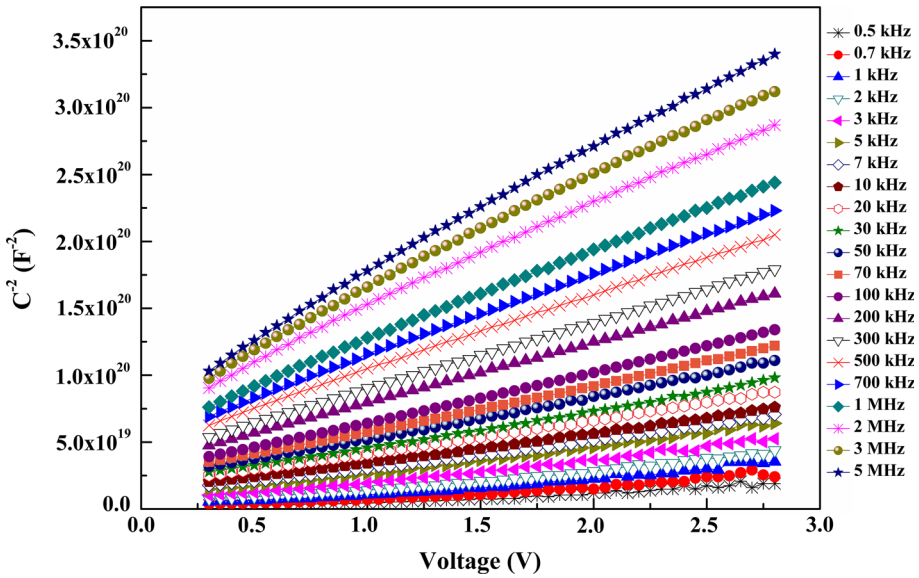

Fig. 9. The C^{-2} versus V plots of the Ag/Ru-doped PVP/n-Si structure for various frequencies at room temperature.

maximum electric field (E_m) were acquired from Eq. 8a. In addition, the BH value (Φ_{C-V}) for Ag/Ru-doped PVP/n-Si structure was obtained using Eq. 8b[24–27]:

$$\Delta\Phi_B = \left[\frac{qE_m}{4\pi\varepsilon_s\varepsilon_0}\right]^{\frac{1}{2}}, E_m = \left[\frac{2qN_DV_0}{\varepsilon_s\varepsilon_0}\right]^{\frac{1}{2}} \quad (8a)$$

Thus, the value of Φ_{C-V} was obtained as a function of frequency:

$$\Phi_{C-V} = \left(V_0 + \frac{kT}{q}\right) + E_F - \Delta\Phi_B = V_D + E_F - \Delta\Phi_B \quad (8b)$$

There is a relationship between the theoretical doping concentration ($N_D = 4.31 \times 10^{15}\text{cm}^{-3}$) and the experimental values of it are known as $c_2 \approx N_D(\text{theor.})/N_D$ (exp.) and it is given in (9)[28–30]:

$$c_2 = 1/((1 + qd_iN_{ss}/\varepsilon_i)) \quad (9)$$

Table II. The frequency-dependent values of V_i, N_D, E_F, E_m, W_D, $\Delta\Phi_B$, $\Phi_{C\text{-}V}$, R_s, c_2, and N_{ss} obtained from the C^{-2}–V plot of the Ag/Ru-doped PVP/n-Si structure at room temperature

Frequency (kHz)	V_i (V)	N_D (cm^{-3})	E_F (eV)	E_m (V/cm)	W_D (cm)	$\Delta\Phi_B$ (eV)	$\Phi_{C\text{-}V}$ (eV)	R_s (Ω)	c_2	N_{ss} (eV^{-1} cm^{-2})
0.5	0.709	1×10^{15}	0.256	1.48×10^{4}	9.61×10^{-5}	4.61×10^{-2}	0.94	19,055	0.233	3.115×10^{12}
0.7	0.602	8.04×10^{14}	0.261	1.22×10^{4}	9.88×10^{-5}	4.19×10^{-2}	0.85	18,702	0.187	4.122×10^{12}
1.0	0.465	6.98×10^{14}	0.265	9.97×10^{3}	9.33×10^{-5}	3.79×10^{-2}	0.72	17,733	0.162	4.894×10^{12}
2.0	0.358	6.13×10^{14}	0.268	8.20×10^{3}	8.73×10^{-5}	3.44×10^{-2}	0.62	14,631	0.142	5.699×10^{12}
3.0	0.175	5.59×10^{14}	0.271	5.49×10^{3}	6.40×10^{-5}	2.81×10^{-2}	0.44	11,001	0.130	6.337×10^{12}
5.0	0.261	6.04×10^{14}	0.269	6.95×10^{3}	7.51×10^{-5}	3.16×10^{-2}	0.52	6555	0.140	5.8002×10^{12}
7.0	0.378	5.73×10^{14}	0.270	8.14×10^{3}	9.28×10^{-5}	3.42×10^{-2}	0.64	4284	0.133	6.169×10^{12}
10	0.469	5.47×10^{14}	0.271	8.87×10^{3}	1.06×10^{-4}	3.57×10^{-2}	0.73	2612	0.127	6.504×10^{12}
20	0.544	4.84×10^{14}	0.274	8.98×10^{3}	1.21×10^{-4}	3.60×10^{-2}	0.81	1089	0.112	7.478×10^{12}
30	0.546	4.40×10^{14}	0.277	8.58×10^{3}	1.27×10^{-4}	3.51×10^{-2}	0.81	739	0.102	8.317×10^{12}
50	0.547	3.83×10^{14}	0.280	8.01×10^{3}	1.37×10^{-4}	3.40×10^{-2}	0.82	513	0.089	9.693×10^{12}
70	0.557	3.50×10^{14}	0.282	7.73×10^{3}	1.44×10^{-4}	3.34×10^{-2}	0.83	435	0.081	1.069×10^{13}
100	0.581	3.19×10^{14}	0.285	7.54×10^{3}	1.54×10^{-4}	3.30×10^{-2}	0.86	376	0.074	1.180×10^{13}
200	0.631	2.68×10^{14}	0.289	7.20×10^{3}	1.75×10^{-4}	3.22×10^{-2}	0.91	280	0.062	1.425×10^{13}
300	0.669	2.44×101^{4}	0.291	7.07×10^{3}	1.89×10^{-4}	3.19×10^{-2}	0.95	229	0.057	1.576×10^{13}
500	0.712	2.16×10^{14}	0.294	6.86×10^{3}	2.07×10^{-4}	3.14×10^{-2}	1.00	175	0.050	1.791×10^{13}
700	0.738	1.99×10^{14}	0.296	6.71×10^{3}	2.20×10^{-4}	3.11×10^{-2}	1.03	148	0.046	1.949×10^{13}
1000	0.754	1.83×10^{14}	0.299	6.50×10^{3}	2.32×10^{-4}	3.06×10^{-2}	1.05	127	0.042	2.137×10^{13}
2000	0.793	1.57×10^{14}	0.302	6.18×10^{3}	2.57×10^{-4}	2.98×10^{-2}	1.09	98	0.036	2.502×10^{13}
3000	0.776	1.42×10^{14}	0.305	5.82×10^{3}	2.67×10^{-4}	2.89×10^{-2}	1.08	84	0.033	2.764×10^{13}
5000	0.737	1.30×10^{14}	0.307	5.41×10^{3}	2.72×10^{-4}	2.79×10^{-2}	1.04	70	0.030	3.046×10^{13}

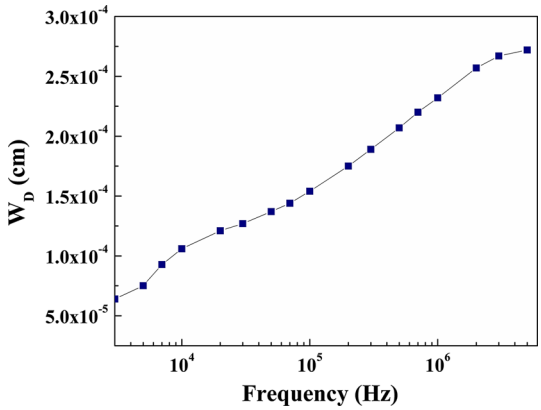

Fig. 10. The frequency-dependent profile of the depletion layer width of the Ag/Ru-doped PVP/n-Si structure at room temperature.

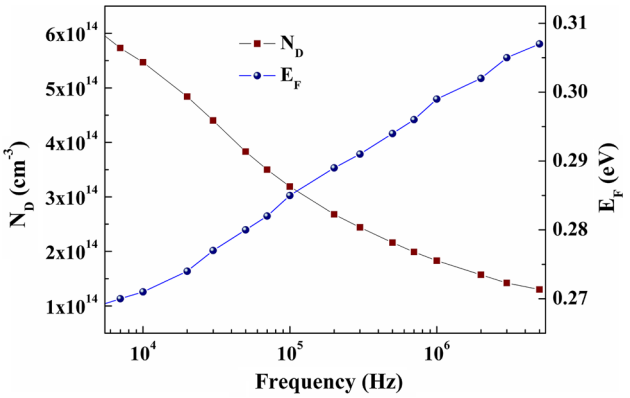

Fig. 11. The frequency-dependent profile of the doping concentration and Fermi energy level in the Ag/Ru-doped PVP/n-Si structure at room temperature.

where d_i is thickness of the interface layer and ε_i is its permittivity. The average density of N_{ss} was obtained from Eq. 9 by taking the d_i value as 100 Å. The values of V_i, N_D, E_F, E_m, W_D, $\Delta\Phi_B$, $\Phi_{C\text{-}V}$, R_s, c_2 and N_{ss} of the Ag/Ru-doped PVP/n-Si structure were measured at room temperature and are given in Table II.

The depletion width (W_D) increases with increasing frequency almost exponentially (Table II and Fig. 10). Otherwise, while the values of E_F increase with increasing frequency, N_D decreases as expected (Fig. 11). Since the surface state charges at high frequencies cannot follow the alternating current (ac) signal, at high frequency, the surface states cannot contribute to the capacitance, contrary to at low frequency. As shown in Fig. 12, the values of $\Phi_{C\text{-}V}$ increase with increasing frequency. These results show that at low frequencies, the nonlinearity of C^{-2}–V plots can be completely clarified based on the assumption that most of surface states can follow the ac signal.

As seen in Tables I and II, the BH values obtained from the reverse-bias C–V characteristics are generally higher than the one obtained from the forward-bias I–V characteristics as well as Fermi energy level (E_F) due to the nature of the measurement method. The reason for this is that the apparent BH of the metal to semiconductor is

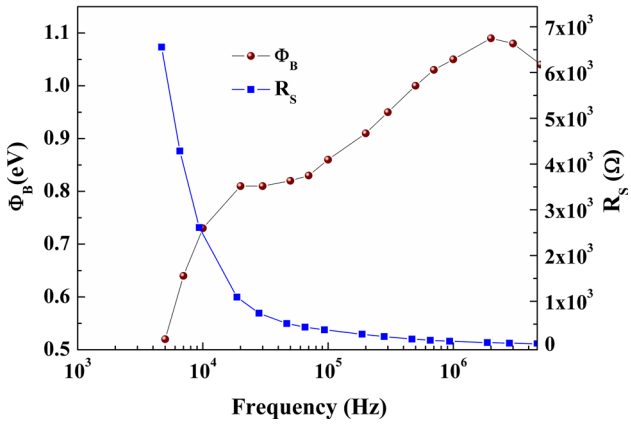

Fig. 12. The frequency-dependent profile of the series resistance (at 5 V) and barrier height in the Ag/Ru-doped PVP/n-Si structure at room temperature.

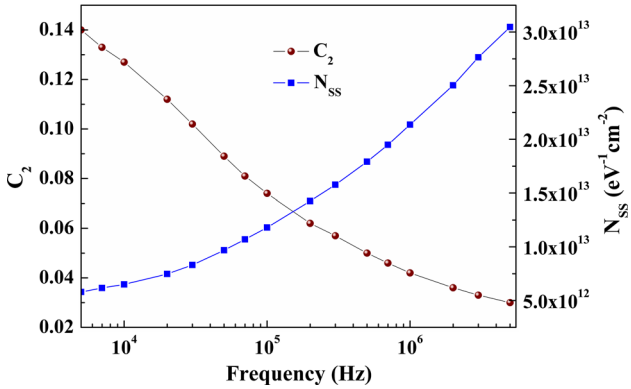

Fig. 13. The frequency-dependent profile of the surface states and c_2 in the Ag/Ru-doped PVP/n-Si structure at room temperature.

always higher than that of the semiconductor to metal as high as the E_F.[18,20] In addition, both C and G are strongly dependent on the frequency in depletion and inversion regions (Figs. 6 and 7). These changes in C and G can be attributed to the ability of the surface states (N_{ss}) to follow the ac signal, density of the surface states and the existence of an interface layer in MS structure.[18,21,24] At low frequencies, the charges at these traps can easily follow the ac signal and yield an excess capacitance and conductance to their measured real values, but at high frequencies, these charges cannot contribute to the C and G, because their relaxation time (τ) is too short for permitting the charge to move in and out of the N_{ss} in response to the ac signal.[18,21,24] However, an interfacial layer easily polarized under an electric field displaces the charges from their equilibrium positions or traps. These charges at the states can easily be attributed to the magnitude of surface and dipole polarization at low and intermediate frequencies.

It is clear that the existence of an interface layer such as an insulator or polymer in MS structure

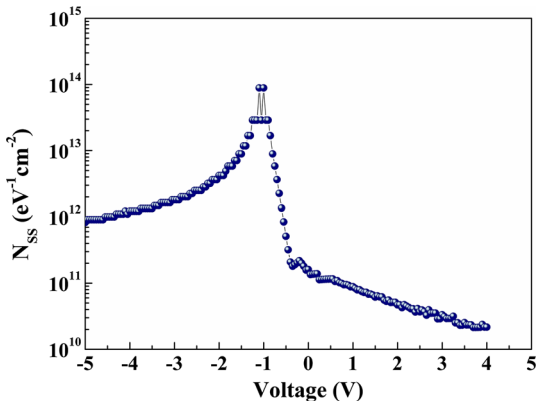

Fig. 14. The surface states versus V plots of the Ag/Ru-doped PVP/n-Si structure for various frequencies at room temperature.

causes the conduction mechanism to differ significantly at a certain temperature, voltage and frequency. In addition, using such a polymer interlayer does not forbid inter-diffusion and reaction between them, but insulates the metal and semiconductor.

In the equal cycle of MIS or MPS structures, the capacitance of the interface layer (C_i) is connected in sequence with the similar combination of the N_{ss} capacitance (C_{ss}) and the space charge capacitance (C_{sc}).[24] On the other hand, the carrier charges at surface states cannot respond to the external ac signal and cannot contribute to the measured capacitance directly. Contrary to the high frequencies, at low frequencies, they can follow this signal well (Fig. 13). Because of this approach, the voltage-dependent profile of N_{ss} can be subtracted from Eq. 10.[24]

$$qAN_{ss} = C_{ss} = \left[(1/C_{LF} - 1/C_i)^{-1} - (1/C_{HF} - 1/C_i)^{-1}\right] \quad (10)$$

The N_{ss}–V plot obtained from Eq. 10 has a distinctive peak at about − 1.15 V. Such behavior of N_{ss}–V can be ascribed to a certain density distribution of surface states between the interface layer and n-Si (Fig. 14).[25–28] The resulting mean value of N_{ss} ($\approx 2 \times 10^{13}$ eV^{-1} cm^{-2}) is more suitable for electronic devices.

CONCLUSION

In order to improve the performance of Ag/n-Si (MS) structure, an Ru-doped PVP interfacial layer was grown between metal and semiconductor by using electrospinning technique. While some of their electrical parameters such as I_o, n, Φ_{Bo}, R_{sh} and RR were obtained from the forward-bias I–V measurements, some of the main parameters such as V_i, N_D, E_F, E_m, W_D, $\Delta\Phi_B$, c_2, Φ_{C-V} and R_s were extracted from the reverse-bias C–V measurements. Furthermore, the energy-dependent profile of N_{ss} was extracted from the forward-bias I–V data by

taking voltage-dependent n and Φ_{B0} values and the high/low-frequency capacitance method, respectively into account. Moreover, the voltage-dependent profile of R_s was obtained from the Ohm's and conductance methods by using I–V and C/G–V measurements, respectively. When all of these parameters are compared to each other, it is inferred that using an Ru-doped PVP interfacial polymer layer plays an important role in improving the quality of MS-type structure, especially in reducing the leakage current, R_s and N_{ss} and increasing the rectifying rate, R_{sh} and BH. The observed abnormal peak in the accumulation region was ascribed to the existence of N_{ss} at the interfacial Ru-doped PVP layer. This peak position shifts toward the positive-bias regions with decreasing frequency. This is because of the fact that the charges at surface states can fully follow the ac signal and yield an excess capacitance (C_{ex}.) and conductance (G_{ex}./). In addition, the observed discrepancy in C–V and G/w–V characteristics with frequency becomes larger in the depletion and the accumulation region, especially at low frequencies because of the existence of charges at surface states localized at the MS interface and their relaxation time and surface polarization. In conclusion, this paper suggests that to increase the performance of MS-type structure, an Ru-doped PVP layer can be used as an interfacial layer instead of conventional insulator layer such as SiO_2 and SnO_2 and TiO_2 in these structures. Prospective studies should focus on a metal-doped polymer insulator layer of MPS structures due to its inexpensive solution processing, good performance, flexibility and low energy expenditure during the production phase.

ACKNOWLEDGEMENTS

This work was supported by ARTEMIZ Research and Development (R&D) Company. ARTEMIZ is an establishment financially supported by the Small and Medium Enterprises Development Organization (KOSGEB), Republic of Turkey.

REFERENCES

1. M. Ravi, Y. Pavani, K. Kiran Kumar, S. Bhavani, A.K. Sharma, and V.V.R. Narasimha Rao. *Mater. Chem. Phys.* 130, 442 (2011).
2. O.G. Abdullah, S.A. Hussen, and A. Alani, *Asian Trans Sci. Technol.* 1, 1 (2011).
3. V. Panwar, C. Lee, S. Young Ko, J. Park, and S. Park, *Mater. Chem. Phys.* 135, 928 (2012).
4. P.R. Sekhar Reddy, V. Janardhanam, I. Jyothi, H.S. Chang, S.N. Lee, M.S. Lee, V.R. Reddy, and C.J. Choi, *Superlattic. Microstruct.* 111, 506 (2017).
5. K. Sreenu, C.V. Prasad, and V.R. Reddy, *J. Electron. Mater.* 46, 5746 (2017).
6. Y. Murakami, P.T. Tue, H. Tsukada, J. Li, and T. Shimoda, *in Proc. of the 20th IDW, Fukuoka* (2013).
7. O. Hinrichsen, F. Rosowski, M. Muhler, and G. Ertl, *Chem. Mater.* 26, 7083 (2014).
8. Y. Xiea and D. Fu, *Mater. Chem. Phys.* 122, 23 (2010).
9. J. Choi, Y. Choi, J. Hong, H. Tian, J. Roh, Y. Kim, T. Chung, Y.W. Oh, Y. Kim, C.G. Kim, and K. No, *Jpn. J. Appl. Phys.* 41, 6852 (2002).
10. A. Gril, W. Kane, J. Viggiano, M. Brady, and R. Laibowitz, *J. Mater. Res.* 7, 3260 (1992).
11. C. Corriol, F. Calleja, A. Arnau, J.J. Hinarejos, A.L. Vázquez de Parga, W.A. Hofer, and R. Miranda, *Chem. Phys. Lett.* 405, 1 (2005).
12. Y.B. He, M. Knapp, E. Lundgren, and H. Over, *J. Phys. Chem B* 108, 14392 (2005).
13. T. Aaltonen, P. Alen, M. Ritala, and M. Leskela, *Chem. Vap. Deposit.* 9, 45 (2003).
14. Y. Murakami, J. Li, and T. Shimoda, *Mater. Lett.* 152, 121 (2015).
15. N. Shiwakoti, A. Bobby, K. Asokan, and B. Antony, *Mater. Sci. Semi. Proc.* 42, 378 (2016).
16. M. M. A. Shirazi, A. Kargari, S. Bazgir, M. Tabatabaei, M. J. A. Shirazi, M.S. Abdullah, T. Matsuura, and A.F. Ismail, *Desalination*, 329 (2013).
17. B.L. Sharma, New York and London, Plenum Press, (1984).
18. S. M. Sze and K. N. Kwok, New Jersey: John Wiley & Sons, (2007).
19. V. R. Reddy, V. Manjunath, V. Janardhanam, Y. Ho-Kil, and C.J. Choi, *J. Electron. Mater.,* 43, 3499 (2014).
20. H.C. Card and E.H. Rhoderick, *J. Phys. D Appl. Phys.* 4, 1589 (1971).
21. E. H. Nicollian, and J.R. Brews, New York: John Wiley and Sons, 117 (1982).
22. L. Rajan, C. Periasamy, and V. Sahula, *Perspect Sci.* 8, 66 (2016).
23. O. Pakma, N. Serin, T. Serin, and Ş. AltındalJ, *Phys. D Appl. Phys.* 41, 215103 (2008).
24. E.H. Rhoderick and R.H. Williams, *Metal-Semiconductor Contacts*, 2nd ed. (Oxford: Clarendon Press, 1978).
25. R. Padma, K. Sreenu, and V. Rajagopal Reddy, *J. Alloy. Compond.* 695, 2587 (2017).
26. M. Sharma and S.K. Tripathi, *Mater. Sci. Semicond. Process.* 41, 155 (2016).
27. S. Kaya and E. Yilmaz, *IEEE Trans. Electron. Dev.* 62, 980 (2015).
28. E.E, Tanrıkulu, D.E. Yıldız, A. Günen, and Ş. Altındal, *Physica Scripta* 90, 095801 (2015).
29. V. Kumar, N. Kaminski, A.S. Maan, and J. Akhtar, *Phys. Status Solidi* 213, 193 (2016).
30. S. Altındal, F. Parlartürk, A. Tataroğlu, M. Parlak, S.N. Sarmasov, and A.A. Agasiev, *Vacuum* 82, 1246 (2008).